A 3D measurement method based on multi-view fringe projection by using a turntable*

SONG Li-mei (宋丽梅)[1]**, **GAO Yan-yan** (高艳艳)[1], **ZHU Xin-jun** (朱新军)[1], **GUO Qing-hua** (郭庆华)[1,2], and **XI Jiang-tao** (习江涛)[2]

1. Key Laboratory of Advanced Electrical Engineering and Energy Technology, Tianjin Polytechnic University, Tianjin 300387, China

2. School of Electrical, Computer and Telecommunications Engineering, University of Wollongong, Wollongong 2500, Australia

(Received 4 July 2016)

In order to get the entire data in the optical measurement, a multi-view three-dimensional (3D) measurement method based on turntable is proposed. In the method, a turntable is used to rotate the object and obtain multi-view point cloud data, and then multi-view point cloud data are registered and integrated into a 3D model. The measurement results are compared with that of the sticking marked point method. Experimental results show that the measurement process of the proposed method is simpler, and the scanning speed and accuracy are improved.

Document code: A **Article ID:** 1673-1905(2016)05-0389-6

DOI 10.1007/s11801-016-6151-x

The three-dimensional (3D) non-contact measurement technology based on structured light has many advantages, such as high speed, low cost and good stability[1]. However, due to shaded light, only a part of the point cloud data for objects' surface can be obtained. In order to obtain the entire point cloud data, multi-angle measurement is needed. At present, the method of sticking marked point is used by the majority objects to reconstruct entire 3D model[2,3]. But for small-size objects, the precision and efficiency of measurement results are low because of the occlusion of the marked point. Therefore, numbers of researches have been devoted to the turntable measurement for obtaining surface measurement of small objects. Park et al[4] put forward a 3D measurement system which used a single-axis turntable as carrier platform. Mohamed and Farouk[5] made a calibration template fixed on the turntable with 45°, and then rotated the turntable with three different angles. Hu et al[6] presented a 3D measurement system based on two-axis turntable with a single charge coupled device (CCD), but the measurement accuracy is not high. Feng et al[7] proposed a method for multi-view measurement based on the two-axis numerical control (NC) turntable by using circular markers. Dai et al[8] proposed two methods to calibrate the revolution axis of 360° based on turntable, and multi-view fringe projection system for surface measurement, however, they didn't employ the two methods to measure small objects.

On the basis of the previous research in our laboratory[9,10], a method based on turntable is proposed to measure small objects. Compared with the above methods, the proposed method solves the problem of measuring small objects. Its operation process is simpler, the scanning speed and accuracy are improved, and the fitting effect is better.

The strategy of 360° surface measurement for small objects adopted in this paper consists of the following steps: (1) camera calibration, (2) turntable calibration, (3) measuring surface in one view with three wavelength phase shift profilometry (TWPSP) method, (4) measuring surface in six views by rotating a turntable and repeating step (3), (5) fitting center in least-squares algorithm, (6) registering the point cloud data from six views. Camera calibration is a primary step for extracting metric information between the 3D object coordinates and the image coordinates. Based on the pinhole camera model and perspective geometry theory[11], a 3D point M is projected to its image point m which can be decomposed as

$$s\overline{m} = \boldsymbol{K}\left[\boldsymbol{R} \quad \boldsymbol{t}\right]\overline{M}, \tag{1}$$

where s is a scale factor, $\boldsymbol{R}=[\boldsymbol{r}_1\ \boldsymbol{r}_2\ \boldsymbol{r}_3]$ and $\boldsymbol{t}$ are the rotation matrix and translation vector, respectively. $\boldsymbol{K}$ is the intrinsic matrix, which is given by

$$\boldsymbol{K} = \begin{bmatrix} \alpha & \gamma & u_0 \\ 0 & \beta & v_0 \\ 0 & 0 & 1 \end{bmatrix}, \tag{2}$$

* This work has been supported by the National Natural Science Foundation of China (Nos.60808020 and 61078041), the Natural Science Foundation of Tianjin City (Nos.15JCYBJC51700 and 16JCYBJC15400), and the National Science and Technology Support (No.2014BAH03F01).

** E-mail: lilymay1976@126.com

where (u_0, v_0) is coordinate of the principal point, α and β are the scale factors for x axis and y axis in the image, and γ is the parameter describing the skew of the two image axes.

Without loss of generality, we assume that Z=0, then Eq.(1) can be expressed as

$$s\begin{bmatrix} x \\ y \\ 1 \end{bmatrix} = \boldsymbol{K}\begin{bmatrix} \boldsymbol{r}_1 & \boldsymbol{r}_2 & \boldsymbol{r}_3 & \boldsymbol{t} \end{bmatrix}\begin{bmatrix} X \\ Y \\ 0 \\ 1 \end{bmatrix} = \boldsymbol{K}\begin{bmatrix} \boldsymbol{r}_1 & \boldsymbol{r}_2 & \boldsymbol{t} \end{bmatrix}\begin{bmatrix} X \\ Y \\ 1 \end{bmatrix}. \tag{3}$$

Meanwhile, we get a homograph matrix as

$$\boldsymbol{H} = \begin{bmatrix} \boldsymbol{h}_1 & \boldsymbol{h}_2 & \boldsymbol{h}_3 \end{bmatrix} = \lambda \boldsymbol{K}\begin{bmatrix} \boldsymbol{r}_1 & \boldsymbol{r}_2 & \boldsymbol{t} \end{bmatrix}. \tag{4}$$

According to the homograph matrix, two constraint equations can be obtained as

$$\begin{cases} \boldsymbol{h}_1^{\mathrm{T}} \boldsymbol{K}^{-\mathrm{T}} \boldsymbol{K}^{-1} \boldsymbol{h}_2 = 0 \\ \boldsymbol{h}_1^{\mathrm{T}} \boldsymbol{K}^{-\mathrm{T}} \boldsymbol{K}^{-1} \boldsymbol{h}_1 = \boldsymbol{h}_2^{\mathrm{T}} \boldsymbol{K}^{-\mathrm{T}} \boldsymbol{K}^{-1} \end{cases}. \tag{5}$$

Let

$$\boldsymbol{B} = \boldsymbol{K}^{-\mathrm{T}} \boldsymbol{K}^{-1} \begin{bmatrix} B_{11} & B_{12} & B_{13} \\ B_{12} & B_{22} & B_{23} \\ B_{13} & B_{23} & B_{33} \end{bmatrix} = \begin{bmatrix} \dfrac{1}{\alpha^2} & -\dfrac{\gamma}{\alpha^2\beta} & \dfrac{v_0\gamma - u_0\beta}{\alpha^2\beta} \\ -\dfrac{\gamma}{\alpha^2\beta} & \dfrac{\gamma^2}{\alpha^2\beta^2} + \dfrac{1}{\beta^2} & -\dfrac{\gamma(v_0\gamma - u_0\beta)}{\alpha^2\beta^2} - \dfrac{v_0}{\beta^2} \\ \dfrac{v_0\gamma - u_0\beta}{\alpha^2\beta} & -\dfrac{\gamma(v_0\gamma - u_0\beta)}{\alpha^2\beta^2} - \dfrac{v_0}{\beta^2} & \dfrac{(v_0\gamma - u_0\beta)^2}{\alpha^2\beta^2} + \dfrac{v_0}{\beta^2} + 1 \end{bmatrix}. \tag{6}$$

We can get five intrinsic parameters of the camera as

$$\begin{cases} \alpha = \sqrt{(B_{33} - [B_{13}^{\ 2} + c_x(B_{12}B_{13} - B_{11}B_{23})]/B_{11})/B_{11}} \\ \beta = \sqrt{\sqrt{(B_{33} - [B_{13}^{\ 2} + c_x(B_{12}B_{13} - B_{11}B_{23})]/B_{11})/B_{11}}/(B_{11}B_{12} - B_{12}^{\ 2})} \\ \mu_0 = -B_{13}\alpha^2/(B_{33} - [B_{13}^{\ 2} + c_x(B_{12}B_{13} - B_{11}B_{23})]/B_{11}) \\ v_0 = (B_{12}B_{13} - B_{11}B_{23})/(B_{11}B_{22} - B_{12}^{\ 2}) \\ \gamma = -B_{12}\alpha^2\beta \end{cases}. \tag{7}$$

External parameters can be calculated by the following formula:

$$\begin{cases} \boldsymbol{r}_1 = \lambda \boldsymbol{K}^{-1} \boldsymbol{h} \\ \boldsymbol{r}_2 = \lambda \boldsymbol{K}^{-1} \boldsymbol{h}_2 \\ \boldsymbol{r}_3 = \boldsymbol{r}_1 \times \boldsymbol{r}_2 \\ \boldsymbol{t} = \lambda \boldsymbol{K}^{-1} \boldsymbol{h}_3 \end{cases}. \tag{8}$$

Because it is difficult to make the rotational axis of turntable parallel to the z axis of base, deterring the rotational axis of the turntable in base is necessary. In order to solve the problem, a criterion sphere mounted on the turntable is used as the calibration tool. Firstly, the light from structured light scanner is projected to the calibration sphere. Secondly, the turntable is rotated in different views, and several parts of the calibration sphere can be obtained. Thirdly, the centers of the calibration sphere are fitted at different views. These centers define a circle, and thus the center point O of the circle can be determined. Finally, joining several parts of the sphere together contrasts to the rotate direction of turntable. By performing the above procedures, the 3D surface information of an object can be measured by the turntable system. The calibration system of the turntable is shown in Fig.1.

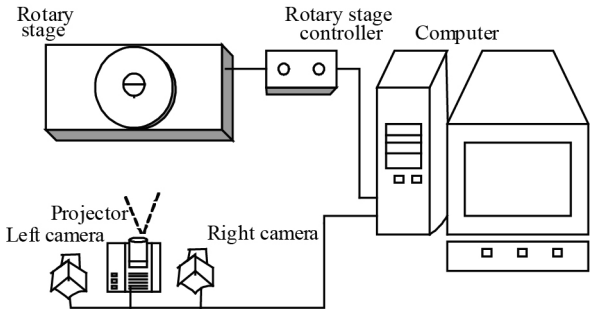

Fig.1 Schematic diagram of the calibration system with turntable

After turntable calibration, all coordinates are transformed into a common coordinate. A TWPSP method[12] for fringe pattern analysis is used to reconstruct the 3D shape, which has been done in the previous research.

W pixels are assumed in the direction vertical to the fringe strips, and three fringe patterns are projected with wavelengths of λ_1 of 1 008 pixels, λ_2 of 144 pixels and λ_3 of 16 pixels, respectively. For every wavelength, the corresponding wrapped phase values of $\varphi_1(x, y)$, $\varphi_2(x, y)$, $\varphi_3(x, y)$ can be calculated in the four steps phase shift profilometry (PSP) algorithm as[13]

$$\varphi_i(x,y) = \arctan\left(\frac{I_0(x,y) - I_2(x,y)}{I_1(x,y) - I_3(x,y)}\right), i = 1,2,3, \tag{9}$$

where $I_K(x, y)$ represents the four pattern images. In order to achieve this, three wavelengths are chosen to meet the following relationships:

$$N_1 = \lambda_1 / \lambda_2 , \quad N_2 = \lambda_2 / \lambda_3 , \tag{10}$$

where N_1 and N_2 must be integers, as $\varphi_1(x, y)$ does not have any discontinuity, there are maximally N_1 discontinuities on $\varphi_2(x, y)$. Also, for each λ_2 pixels on $\varphi_3(x, y)$, there are N_2 discontinuities. Therefore, in total there are maximally $N_1 \times N_2$ discontinuities on $\varphi_3(x, y)$, which can be eliminated by phase unwrapping operation below, yielding the absolute phase $\Phi_3(x, y)$ as

$$\begin{aligned}&\Phi_3(x,y)=\varphi_3(x,y)+\\&2\pi\left\{\mathrm{int}\left[\frac{\varphi_1(x,y)}{2\pi/N_1}\right]\times N_2+\mathrm{int}\left[\frac{\varphi_2(x,y)}{2\pi/N_2}\right]\right\}=\\&\varphi_3(x,y)+\\&2\pi\left\{\mathrm{int}\left[\frac{\varphi_1(x,y)}{2\pi}\times N_1\right]\times N_2+\mathrm{int}\left[\frac{\varphi_2(x,y)}{2\pi}\times N_2\right]\right\}.\end{aligned}\tag{11}$$

Note that when $\varphi_3(x, y)=2\pi$, a discontinuity will occur. In order to remove such a discontinuity, the phase unwrapping equation of $\Phi_3(x, y)$ should be revised to

$$\Phi_3(x,y)=\begin{cases}\varphi_3(x,y)+2\pi\left\{\mathrm{int}\left[\dfrac{\varphi_1(x,y)}{2\pi}\times N_1\right]\times\right.\\\qquad\left.N_2+\mathrm{int}\left[\dfrac{\varphi_2(x,y)}{2\pi}\times N_2\right]\right\},\\\varphi_3(x,y)\neq 2\pi \text{ and } \varphi_2(x,y)\neq\\\qquad 2\pi \text{ and } \varphi_1(x,y)\neq 2\pi\\\varphi_3(x,y)+2\pi\left\{\mathrm{int}\left[\dfrac{\varphi_1(x,y)}{2\pi}\times N_1\right]\times\right.\\\qquad\left.N_2+\mathrm{int}\left[\dfrac{\varphi_2(x,y)}{2\pi}\times N_2\right]-1\right\},\\\varphi_3(x,y)=2\pi \text{ or } \varphi_2(x,y)=\\\qquad 2\pi \text{ and } \varphi_1(x,y)\neq 2\pi\\\varphi_3(x,y)+2\pi\left\{\mathrm{int}\left[\dfrac{\varphi_1(x,y)}{2\pi}\times N_1-1\right]\times\right.\\\qquad\left.N_2+\mathrm{int}\left[\dfrac{\varphi_2(x,y)}{2\pi}\times N_2\right]\right\},\\\varphi_3(x,y)\neq 2\pi \text{ and } \varphi_2(x,y)\neq\\\qquad 2\pi \text{ and } \varphi_1(x,y)=2\pi\end{cases}\tag{12}$$

After the measurement of binocular scanner, a lot of 3D points are obtained, and the least-squares algorithm[14] is needed to fit the center. The center coordinate of calibration ball is set as $M_0(x_0, y_0, z_0)$, and the radius is r. $M_i(x_i, y_i, z_i)$ are obtained from the measurement with structured light scanner.

The algebraic residuals of $M_0(x_0, y_0, z_0)$ and the measurement points $M_i(x_i, y_i, z_i)$ is

$$l_i = (x_i - x_0)^2 + (y_i - y_0)^2 + (z_i - z_0)^2 - r^2 . \tag{13}$$

The objective function based on the residuals is

$$J = \sum_{i=1}^{N} \frac{1}{2} (\|M_i - M_0\| - r)^2 . \tag{14}$$

It can obtained by derivation of the objective function that

$$\frac{\partial J}{\partial r} = \sum_{i=1}^{N} (r - \|M_i - M_0\|) = 0 , \tag{15}$$

$$\frac{\partial J}{\partial x} = \sum_{i=1}^{N} (x_0 - x_i)(1 - \frac{r}{\|M_i - M_0\|}) = 0 , \tag{16}$$

$$\frac{\partial J}{\partial y} = \sum_{i=1}^{N} (y_0 - y_i)(1 - \frac{r}{\|M_i - M_0\|}) = 0 , \tag{17}$$

$$\frac{\partial J}{\partial z} = \sum_{i=1}^{N} (z_0 - z_i)(1 - \frac{r}{\|M_i - M_0\|}) = 0 . \tag{18}$$

Eqs.(15)—(18) are composed of nonlinear equations, and $M_0(x_0, y_0, z_0)$ and the radius can be obtained through the solution of nonlinear equations.

Fig.2 shows the structure of binocular structured light 3D measurement system. It consists of two CCD cameras with pixel of 1 280×1 024 and a projector. In this measurement system, the binocular structured light 3D measurement system is positioned in the front of the calibration template, and two cameras are used to capture at least five images from different directions. The plane circle is taken as calibration template, and the center of characteristic circle is treated as the point of calibration.

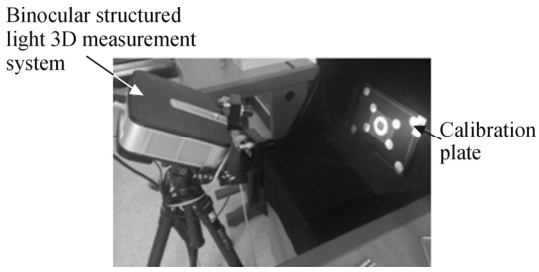

Fig.2 The structure of experimental system for camera calibration

Fig.3 shows the structure of binocular structured light 3D scanner and turntable system. The calibration ball is fixed on the zero scale of the turntable, the rotation of the turntable is controlled by motor controller, and it is rotated 60° once in the measurement process. The specific process of the turntable calibration is as follows. (1) The turntable is resettled at zero scale. (2) The calibration ball is mounted on the turntable and rotated along the axis of rotation. The measurement is carried out from 6 different angles. (3) The noise of the point cloud data are removed

from different angles respectively. (4) The centers of point cloud data are fitted from six perspectives, and the calibration is ending, the axis is shown in Fig.4. (5) The centers obtained from step (4) define a circle, and the circle is fitted in the opposite direction of rotation. The fitting effect of the calibration ball is shown in Fig.5.

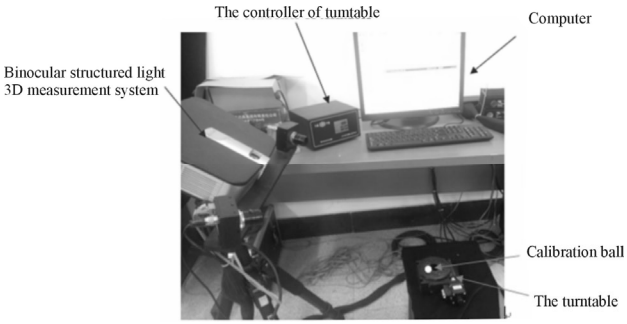

Fig.3 Photo of turntable calibration system

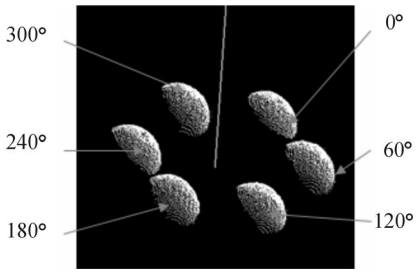

Fig.4 The display of point cloud data from 6 perspectives

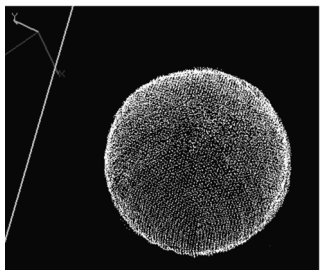

Fig.5 The fitting effect of the calibration ball

Cam is extensively used in the field of machinery. Its main function is to help the follower lever complete a variety of complex movement in accordance with the requirements of the work, including linear motion, swing and variable-speed motion. The function of the cam is realized through its profile. However, we know from Fig.6 that the cam has small size and special requirements on surface, and it is very difficult to measure. Traditionally, cam was measured by special instrument with the contact, which leads to slow speed and high cost. Therefore, the proposed method is used to measure the cam.

After completing the turntable calibration, the vision coordinate and turntable coordinate are combined together. In order to obtain better measurement results, the TWPSP method was used to measure the cam. The wrapped phase maps of cam with three wavelengths are shown in Fig.7.

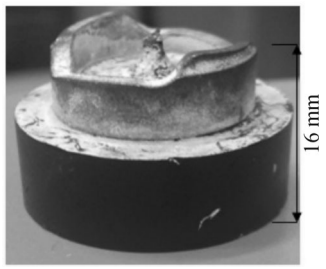

Fig.6 The size and profile of the cam

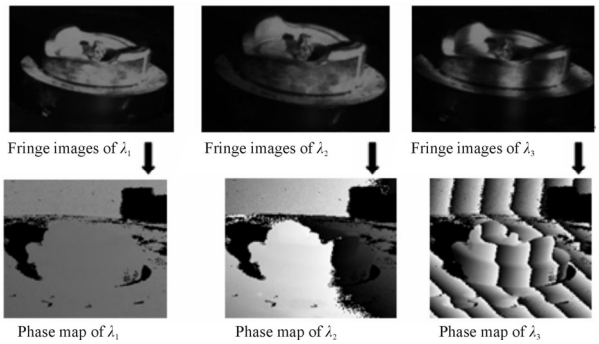

Fig.7 The wrapped phase maps of cam from the TWPSP method

Now let us consider a row of pixels in the fringe images on the row 512. In the experiments, Fig.8(a)—(c) show the wrapped phases of cam with wavelengths of λ_3, λ_2 and λ_1 from the TWPSP method, respectively.

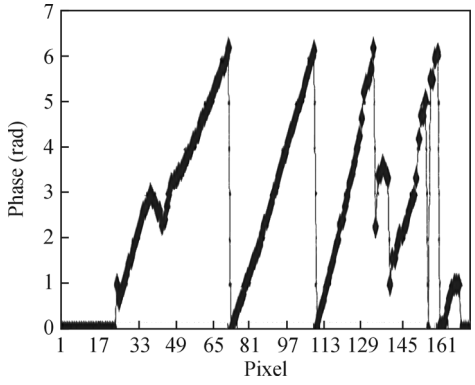

(a) The wrapped phase of λ_3 from the TWPSP method

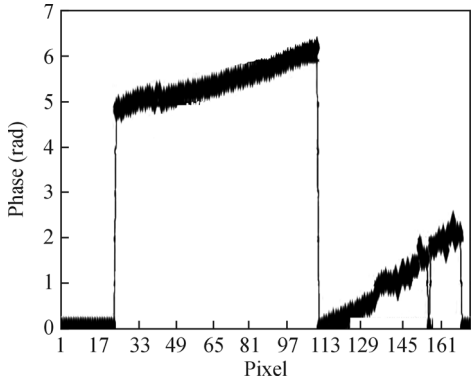

(b) The wrapped phase of λ_2 from the TWPSP method

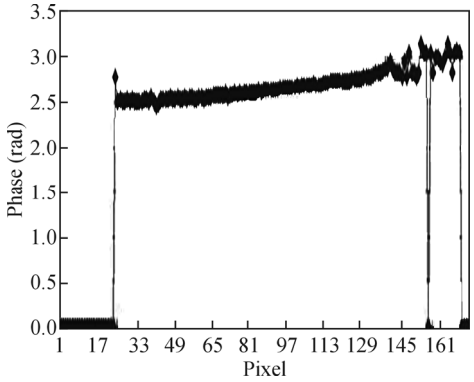

(c) The wrapped phase of λ_1 from the TWPSP method

Fig.8 The wrapped phase of cam with wavelengths of λ_3, λ_2 and λ_1 from the TWPSP method

In order to demonstrate the advantages of the proposed method, the sticking marked point method is also used for comparison. The form of marked point is a black circle, which is pasted on the surface of the object as shown in Fig.9(b).

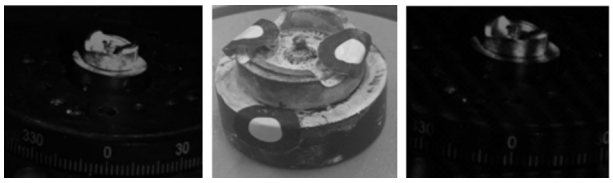

(a) The proposed method (b) The sticking marked point method (c) Projected fringe patterns of cam

Fig.9 Two methods for measuring the cam

When the sticking marked point method is used, all point clouds in different views are shown in Fig.10.

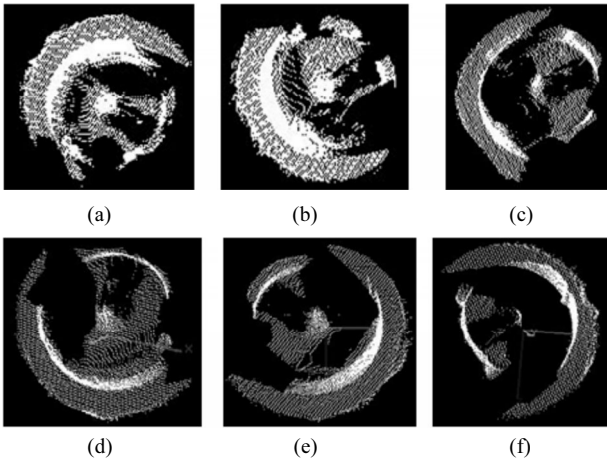

(a) (b) (c)

(d) (e) (f)

Fig.10 Point cloud data of cam from 6 views

When the proposed method is used, the cam is placed on the 0 scale of turntable and measured every 60°. All point cloud data in different views are shown in Fig.11.

Then register these multi-view point cloud data and compare the fitting effects of these two methods. The fitting effects of two methods are shown in Fig.12.

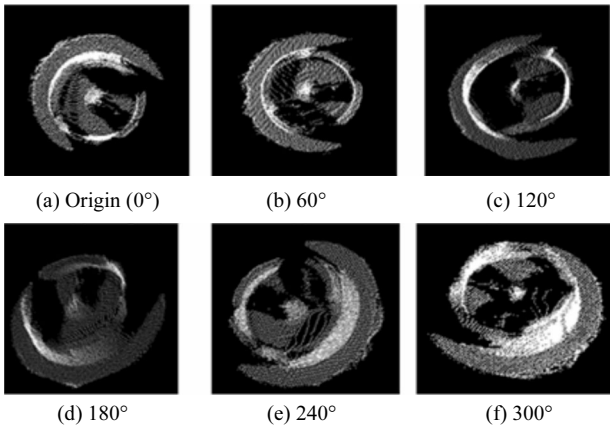

(a) Origin (0°) (b) 60° (c) 120°

(d) 180° (e) 240° (f) 300°

Fig.11 Point cloud data of cam measured every 60°

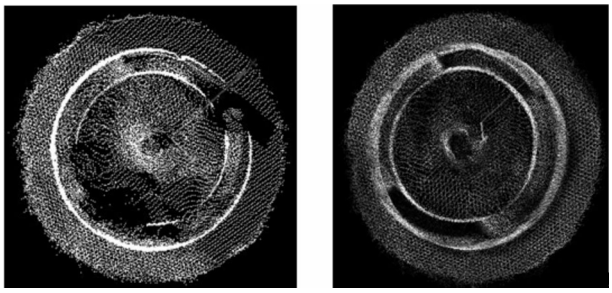

(a) (b)

Fig.12 The fitting effect of cam in (a) sticking marked point method and (b) the proposed method

From the results of two methods, it can be found that the proposed method is well reconstructed, the entire point cloud data can be obtained, and the fitting effect is better. However, in the method of sticking marked point, many important point clouds are lost, and the fitting effect is also incomplete.

The statistical results of two methods are shown in Tab.1, and the error analyses of two methods are shown in Fig.13. We can see that the time of the proposed method is about 100 s (including the turntable calibration), and the total process is without manual involvement, what we should do is just placing the cam on the turntable. The time of the sticking marked point method is 5 min, and the process is with a lot manual work, such as pasting and cleaning the markers. So the proposed method is faster and simpler, moreover, the measurement error of the proposed method is smaller than that of the sticking marked point method.

Tab.1 The statistics results of the two methods

Parameters	The proposed method	The sticking marked point method
The average number of point cloud from six views	9 273	7 085
Mean error (mm)	0.227	0.235
Standard deviation (mm)	0.168	1.079
Time (s)	100	300

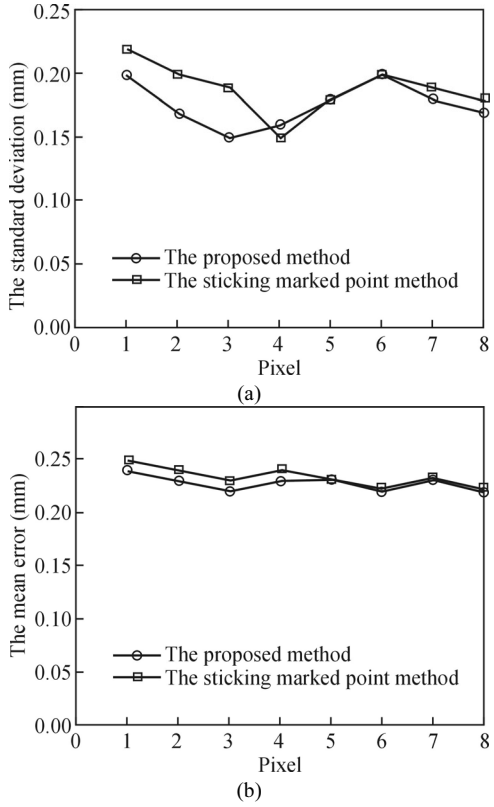

Fig.13 (a) The standard deviation and (b) the mean errors of the two methods

A 3D measurement method based on turntable system is proposed to measure small objects in this paper. Firstly, camera and turntable are calibrated. Secondly, a turntable stage is employed to rotate the object, and multi-view point cloud data are obtained. Finally, Multi-view point cloud data are then registered and integrated into a 3D model. Through comparing the sticking marked point method with the proposed method, the advantages of the proposed method can be summarized as follows. Firstly, the measurement process is simpler. Secondly, the problem of measuring small objects with small surface area and special requirements on the surface is solved. Thirdly, the accuracy is higher, and the fitting effect is better.

Acknowledgments

We thank the National Natural Science Foundation Committee and the Tianjin Research Program of Application Foundation and Advanced Technology for the support. This research is also supported by the State Key Laboratory of Precision Measuring Technology and Instruments (Tianjin University).

References

[1] J. Geng, Advances in Optics and Photonics **3**, 128 (2011).

[2] L. M. Zhou, X. H. Zhang and B. L. Guan, Measurement **58**, 115 (2014).

[3] X. L. Liu, X. Peng, H. L. Chen, D. He and B. Z. GAO, Optics Letters **37**, 3126 (2012).

[4] S. Y. Park and M. Subbarao, Machine Vision and Applications **16**, 148 (2005).

[5] M. Farouk, I. El-Rifai, S. El-Tayar, H. El-Shishiny, M. Hosny, M. El-Rayes, J. Gomes, F. Giordano, H. Rushmeier, F. Bernardini and K. Magerlein, Scanning and Processing 3D Objects for Web Display, IEEE 4th International Conference on 3D Digital Imaging and Modeling, 310 (2003).

[6] M. Hu and J. Xi, Journal of Shanghai Jiao Tong University **44**, 506 (2010).

[7] H. Feng, L. Zhang, X. Wang and H. Wang, Mechanical Science and Technology for Aerospace Engineering **31**, 244 (2012). (in Chinese)

[8] M. Dai, L. Chen, F. Yang and X. He, Applied Optics **52**, 5440 (2013).

[9] L. M. Song, P. Q. Wang, Y. L. Chang, X. J. Li, J. T. Xi, Q. H. Guo and B. N. Li, Optoelectronics Letters **11**, 145 (2015).

[10] L. M. Song, D. P. Li, M. C. Qin, Z. Y. Li, Y. L. Chang and J. T. Xi, Optoelectronics Letters **10**, 378 (2014).

[11] Z. Y. Zhang, IEEE Transaction Pattern Analysis and Machine Intelligence **22**, 1330 (2000).

[12] L. M. Song, Y. L. Chang, J. T. Xi, Q. H. Guo, X. J. Zhu and X. J. Li, Optics Communications **355**, 213 (2015).

[13] L. M. Song, X. X. Dong, J. T. Xi, Y. G. Yu and C. K. Yang, Optics & Laser Technology **45**, 319 (2013).

[14] S. Theodoridis, The Least-Squares Family, 6th ed., Academic Press, Oxford, 2015.